Supplementary Information for: Attributing Venice Acqua Alta events to a changing climate and evaluating the efficacy of MoSE adaptation strategy

Davide Faranda[1,2,3*], Mireia Ginesta[1], Tommaso Alberti[4], Erika Coppola[5], Marco Anzidei[4]

[1*]Laboratoire des Sciences du Climat et de l'Environnement, CEA Saclay l'Orme des Merisiers, UMR 8212 CEA-CNRS-UVSQ, Gif-sur-Yvette, 91191, France.
[2]London Mathematical Laboratory, 8 Margravine Gardens, London, W6 8RH, UK.
[3]Laboratoire de Météorologie Dynamique/IPSL, École Normale Supérieure, PSL Research University, Sorbonne Université, 75005, Paris, France, École Polytechnique, IP Paris, Paris, 75005, France.
[4]Istituto Nazionale di Geofisica e Vulcanologia, via di Vigna Murata 605, Rome, 00143, Italy.
[5]International Centre for Theoretical Physics, Strada Costiera 11, Trieste, 34100, Italy.

*Corresponding author(s). E-mail(s): davide.faranda@lsce.ipsl.fr; Contributing authors: mireia.ginesta@lsce.ipsl.fr; tommaso.alberti@ingv.it; coppolae@ictp.it; marco.anzidei@ingv.it;

Abstract

The supplementary material of this paper provides additional detailed analyses of the extreme flooding events that occurred in Venice in 1966, 2008, 2018 and 2019. The material includes detailed methodological element, explanation and figures that show the temporal evolution of sea-level pressures, temperatures, precipitations, wind speed of the four events analysed. Additionally, the material provides detailed information on the sea-level and the estimated damages caused by the flooding, including the affected area for 2008, 2018 and 2019. The supplementary material also includes details about the 2008, 2018 and 2019 events and a comparison with the 1966 Great Flood of Venice, highlighting similarities and differences in terms of sea level, storm surge, and damage.

Keywords: Climate Change, Attribution, Sea Level, Adaptation, Mitigation

1 Supplementary Methods

Analogue quality Q

Q is the average Euclidean distance of a given day from its 17 closest analogues. If the value of Q for the extreme event belongs to the same distribution of its analogues then the event is not unprecedented and the attribution can be performed, if the value of Q is greater than those of its analogues the event is unprecedented and therefore not attributable.

Predictability Index D

Using dynamical systems theory [1–3], we can compute the local dimension D of each slp map [4, 5]. The local dimension is a proxy for the number of degrees of freedom of the field, meaning that the higher D, the more unpredictable the temporal evolution of the slp maps will be [6–8]. If the dimension D of the analyzed event is higher or lower than that of its analogues, then the extreme will be respectively less or more predictable than the closest dynamical situations identified in the data. The concept of dimension D is strictly related to that of attractor for a dynamical system, i.e., a geometric object defined in the space hosting all the possible states of the system (phase-space). Each point ζ on the attractor can be characterized by two dynamical indicators: the local dimension D, which indicates the number of degrees of freedom active locally around ζ, and the persistence Θ, a measure of the mean residence time of the system around ζ [6, 9]. To determine D, we exploit recent results from the application of extreme value theory to Poincaré recurrences in dynamical systems. This approach considers long trajectories of a system — in our case successions of slp latitude–longitude maps — corresponding to a sequence of states (in time) on the attractor. For a given point ζ in phase-space (e.g., a given slp map), we compute the probability that the system returns within a ball of radius ϵ centered on the point ζ. The Freitas et al. [10] theorem, modified by Lucarini et al. [11], states that logarithmic returns:

$$g(x(t)) = -\log(\mathrm{dist}(x(t), \zeta)) \tag{1}$$

yield a probability distribution such that:

$$\Pr(z > s(q)) \simeq \exp\left[-\vartheta(\zeta)\left(\frac{z-\mu(\zeta)}{\sigma(\zeta)}\right)\right] \tag{2}$$

where $z = g(x(t))$, s is a high threshold associated to a quantile q of the series $g(x(t))$, and $\vartheta(\zeta)$ the extremal index [12]. Requiring that the orbit falls within a ball of radius ϵ around the point ζ is equivalent to asking that the series $g(x(t))$ is over the threshold s; therefore, the ball radius ϵ is simply $e^{-s(q)}$. The resulting distribution is the exponential member of the Generalized Pareto Distribution family. The parameters μ and σ, namely the location and the scale parameter of the distribution, depend on the point ζ in phase space. $\mu(\zeta)$ corresponds to the threshold $s(q)$ while the local dimension $D(\zeta)$ can be obtained via the relation $\sigma = 1/D(\zeta)$.

When $x(t)$ contains all the variables of the system, the estimation of D based on extreme value theory has a number of advantages over traditional methods (e.g. the box counting algorithm [13, 14]). First, it does not require to estimate the volume of different sets in scale-space: the selection of $s(q)$ based on the quantile provides a selection of different scales s which depends on the recurrence rate around the point ζ. Moreover, it does not require the a priori selection of the maximum embedding dimension as the observable g is always a univariate time-series.

Persistence Index Θ

The persistence of the state ζ is measured via the extremal index $0 < \vartheta(\zeta) < 1$, a dimensionless parameter, from which we extract $\Theta(\zeta) = \Delta t/\vartheta(\zeta)$. Here, Δt is the timestep of the dataset being analysed. $\Theta(\zeta)$ is therefore the average residence time of trajectories around ζ, namely the metric of persistence introduced in Section 1, and it has unit of a time (in this study days). If ζ is a fixed point of the attractor, then $\Theta(\zeta) = \infty$. For a trajectory that leaves the neighborhood of ζ at the next time iteration, $\Theta = 1$. To estimate ϑ, we adopt the Süveges estimator [12]. For further details on the the extremal index, see Moloney et al. [15].

Assessing the role of Natural Variability

We consider the possible roles of the El Niño-Southern Oscillation (ENSO), North Atlantic Oscillation (NAO), the Pacific Decadal Oscillation (PDO) and the Atlantic Multidecadal Oscillation (AMO) in affecting the analysed extreme events. We perform this last analysis using monthly indices NOAA/NCEP/CPC, the PDO/SWSFC (Southwest Fisheries Science Center), the NINO34/ERSSTv5 and the AMO/ERSSTv5 data and retrieved from the Royal Netherlands Meteorological Institute (KNMI) Climate Explorer. In particular, the ENSO index is version 3.4 as defined by [16], the PDO and the AMO index is calculated as described in [17]. When the ENSO 3.4 index is positive, it corresponds to El Niño, and when it is negative, it corresponds to La Niña. To assess the possible association of ENSO and AMO on circulation changes between factual and counterfactual periods, we compare the distributions of indices for the analogues of the two periods and we evaluate any significance changes between factual and counterfactual distributions by performing a two-tailed Cramér-von Mises test [18] at the 0.05 significance level. If the p-value is smaller than 0.05, the null hypothesis that both samples are from the same distribution is rejected, and the influence of internal variability cannot be excluded. All relevant figure panels display the p-value (pval) in the title.

2 Supplementary Notes

Additional Analyses for the 1966 event

The quality of the analogues (Supplementary Figure 1a) shows that this circulation is extremely uncommon compared to the rest of the analogues with no significant changes in the two periods. We do not detect significant increases neither in predictability D (Supplementary Figure 1b) nor in persistence Θ for both present and past periods (Supplementary Figure 1c). The seasonal occurrence of analogues (Supplementary Figure 1d) shows a shift towards the month of November in the present period. This explain why we do not observe a warming signal in Supplementary Figure 1. We mostly ascribe changes to human-driven climate change, as natural climate variability likely played a modest role (see Supplementary Figure 8).

Analyses for the 2008 event

On December 1, 2008, at 10:45 am, Venice experienced an exceptionally high tide of 156 cm, ranking as the fourth-highest recorded in tidal surveys. This surge was primarily attributed to meteorological factors, with nearly one meter of the increase attributable to a rapid drop in atmospheric pressure and the presence of a strong Scirocco wind in both Venice and the wider Adriatic region. These meteorological conditions almost perfectly coincided with the expected astronomical high tide. Examining the data, it becomes evident a depression of the atmospheric pressure in Venice by approximately 13 hPa over the course of 9 hours. Additionally, wind direction shifted abruptly from the north-northeast to a Scirocco wind pattern, with wind speeds ranging from 40 to 80 km/h, lasting for the subsequent 7-8 hours. The following day, a secondary event occurred, albeit with reduced intensity, as meteorological conditions had started to improve on the afternoon of December 1. At 10:45 am, a lower sea level of 102 cm has been measured.

Supplementary Figure 2 shows the results of the attribution of the synoptic configuration associated with the event. The domain analyzed is 5°E-16°W 40°N-49°N. The slp field of the event (Supplementary Figure 2a) has been used for the search of 17 analogues for the past and present periods. Their average is displayed in Supplementary Figure 2b,c), respectively. We observe significant differences in the pressure field when subtracting present from past analogues leading to more anticyclonic conditions in the present (Supplementary Figure 2d). The atmospheric pattern of the present period is further associated with higher temperatures over the Alps (Supplementary Figure 2e-h) and higher precipitation over the Tyrrhenian sea (Supplementary Figure 2i-l). Winds (Supplementary Figure 2m-p) are generally stronger on the Tyrrhenian sea but not on the Adriatic. The quality of the analogues (Supplementary Figure 5a) shows that this circulation is relatively rare – but less than the 1966 event– when compared to the rest of the analogues with no significant changes in the two periods. We do not detect visible changes in predictability D (Supplementary Figure 5b) nor in persistence Θ (Supplementary Figure 5c) relative to the past world by half of the day. The seasonal occurrence of analogues (Supplementary Figure 5d) does not present any significantly shifts from past to present period. We mostly ascribe changes to human-driven climate change, as natural climate variability likely played a modest role (see Supplementary Figure 8).

Analyses for the 2018 event

On Monday, October 29, 2018, at 2:40 pm, the tide reached a value of 156cm in Punta Salute, Venice, causing significant flooding (https://www.comune.venezia.it/it/content/le-acque-alte-eccezionali#29ottobre). The event was partly caused by an Atlantic disturbance that remained stable between the Gulf of Lyon and the Gulf of Genoa, but the effects were amplified by two blocking anticyclones positioned in Eastern Europe and the Azores [19]. The anticyclones caused a strong acceleration of the southerly winds along the Adriatic coast. On Monday, the atmospheric pressure in Venice dropped by 12 hPa in 16 hours. The southerly wind had been blowing since Sunday, reaching an average speed of around 60km/h and gusts of up to 95km/h. The wind blew violently in the lagoon, especially when a convective thunderstorm generated over Venice in the evening. The intense gusts raised internal waves in the main canals of the city and islands, causing significant damage to the barriers, including those protecting the tide center, residential buildings, and commercial activities. The flooding covered 73% of the pedestrian areas and ranked fourth in importance, equaled with the level reached on December 1, 2008. The lowest level was 119cm at 5:35 pm, the highest in history, except for the 1966 event, which registered 116cm. In the evening, the maximum was 148cm at 8:25 pm, ranking seventh in height and covering about 65% of the Venice's walkable surface. The consecutive presence of the sea level above 120cm was approximately 14 hours, equaling the 1966 record.

Supplementary Figure 3 shows the results of the attribution of the synoptic configuration associated with the episode. The domain analyzed is 5°E-16°W 32°N-45°N. The slp field of the event (Supplementary Figure 3a) has been used for the search of 17 analogues for the past and present periods. Their average is displayed respectively in Supplementary Figure 3b,c). We observe significant differences in the pressure field when subtracting present from past analogues leading to more anticyclonic conditions in the present (Supplementary Figure 3d). The atmospheric pattern of the present period is further associated with higher temperatures over the Eastern Alps (Supplementary Figure 3e-h) and higher precipitation over Liguria and Lombardia (Supplementary Figure 3i-l). Winds (Supplementary Figure 3m-p) are generally stronger on the Tyrrhenian sea and on the Adriatic possibly increasing the risks for the city of Venice. The quality of the analogues (Supplementary Figure 6a) shows that this circulation is relatively rare – but less than the 1966 event– when compared to the rest of the analogues with no significant changes in the two periods. We do not detect visible changes in predictability D (Supplementary Figure 6b) nor in persistence Θ (Supplementary Figure 6c) relative to the past world by half of the day. The seasonal occurrence of analogues (Supplementary Figure 6d) does not present any significantly shifts from past to present period. We ascribe these changes to a mixture of human-driven climate change and natural climate variability as ENSO and AMO distributions have significantly changed between past and present periods (see Supplementary Figure 8).

Analyses for the 2019 event

To understand the causes of the Aqua Granda phenomenon that occurred on November 12th, we needed to reconstruct the meteorological situation of that day, which developed within the framework of the particular meteorological situation of the entire month (https://www.comune.venezia.it/it/content/le-acque-alte-eccezionali#12novembre2019). We have come to the conclusion that the exceptional levels of high tide recorded on November 12, 2019, cannot be attributed solely to the Scirocco wind blowing in the Adriatic Sea [19, 20]. A comparison with the Vaia storm that occurred on October 29, 2018, shows that although the meteorological contribution in 2018 was much greater, the maximum contribution occurred during a minimum astronomical tide. On the other hand, in the case of the unfortunate coincidence of November 12th, 2019, the peak of the meteorological contribution coincided perfectly with the peak of the astronomical tide [19, 21].

Moreover, the strength of the local wind was also unusual, due to an exceptional meteorological situation [19, 22]. Our detailed analysis of the dynamics of atmospheric circulation can help to understand what happened on the evening of November 12th. From November 11th to 12th, the movement of the depression center towards the southern Tyrrhenian Sea induced Scirocco winds along the Adriatic, but limited to the central basin. Persistent winds from the north, northeast with average speeds of up to 14 m/s were present in the northern Adriatic. On November 12, the movement towards the northeast of the main pressure minimum present over the Tyrrhenian Sea caused the formation of a secondary minimum on the Adriatic, downwind of the Umbro-Marchigiano Apennines. This is an event similar, on a smaller scale, to the much more common formation of a cyclone on the Gulf of Genoa as a result of the interaction between a low pressure system coming from the west and the Alpine relief (the so-called "Alpine cyclogenesis"): an occasionally observed meteorological phenomenon in the Upper Adriatic, both in terms of spatial and temporal dimensions, and with an equally unusual evolution. In the afternoon, this local depression moved northwestward to the Upper Adriatic, generating a reinforcement of winds from the Bora and Scirocco during its ascent from Marche to Veneto.

Supplementary Figure 4 shows the results of the attribution of the synoptic configuration associated with the 2019 episode. The domain analyzed is 5°W-16°W 39°N-48°N. The slp field of the event (Supplementary Figure 4a) has been used for the search of 17 analogues for the counterfactual and factual periods. Their average is displayed respectively in Supplementary Figure 4b,c). We observe no significant differences in the pressure field when subtracting present from past analogues leading to more anticyclonic conditions in the present (Supplementary Figure 4d). Temperature maps show no significant changes between past and present periods (Supplementary Figure 4e-h). The analysis for precipitation data shows higher precipitation over Tuscany, Friuli and Istria (Supplementary Figure 4i-l). Winds (Supplementary Figure 4m-p) are generally stronger altough results are significant only in limited areas. The quality of the analogues (Supplementary Figure 7a) shows that this circulation is extremely rare, compared to the rest of the analogues with no significant changes in the two periods. The pattern of 2019 event is therefore unprecedented. We do not detect visible changes in predictability D (Supplementary Figure 6b) nor in persistence Θ (Supplementary Figure 6c) relative to the past world by half of the day. The seasonal occurrence of analogues (Supplementary Figure 6d) shifts from October to November in the present period. This can explain why the signal for temperature changes is rather weak. Finally, we ascribe these changes mostly to human-driven climate change as just the AMO natural has significantly changed between past and present periods (see Supplementary Figure 8).

References

[1] Freitas, A.C.M., Freitas, J.M., Todd, M.: Extreme value laws in dynamical systems for non-smooth observations. J. Stat. Phys. **142**(1), 108–126 (2011)

[2] Freitas, A.C.M., Freitas, J.M., Vaienti, S.: Extreme Value Laws for sequences of intermittent maps. arXiv preprint arXiv:1605.06287 (2016)

[3] Lucarini, V., *et al.*: Extremes and Recurrence in Dynamical Systems. John Wiley & Sons, ??? (2016)

[4] Faranda, D., Messori, G., Alvarez-Castro, M.C., Yiou, P.: Dynamical properties and extremes of Northern Hemisphere climate fields over the past 60 years. Nonl. Proc. Geophy. **24**(4), 713–725 (2017)

[5] Faranda, D., Messori, G., Vannitsem, S.: Attractor dimension of time-averaged climate observables: insights from a low-order ocean-atmosphere model. Tellus A **71**(1), 1–11 (2019)

[6] Faranda, D., Messori, G., Yiou, P.: Dynamical proxies of north atlantic predictability and extremes. Sci. Rep. **7**, 41278 (2017)

[7] Messori, G., Caballero, R., Faranda, D.: A dynamical systems approach to studying midlatitude weather extremes. Geophys. Res. Lett. **44**(7), 3346–3354 (2017)

[8] Hochman, A., Alpert, P., Harpaz, T., Saaroni, H., Messori, G.: A new dynamical systems perspective on atmospheric predictability: Eastern mediterranean weather regimes as a case study. Sci. Adv. **5**(6), 0936 (2019)

[9] Alberti, T., Faranda, D., Lucarini, V., Donner, R.V., Dubrulle, B., Daviaud, F.: Scale dependence of fractal dimension in deterministic and stochastic Lorenz-63 systems. Chaos **33**(2), 023144 (2023)

[10] Freitas, A.C.M., Freitas, J.M., Todd, M.: Hitting time statistics and extreme value theory. Prob. Th. Rel. Field. **147**(3-4), 675–710 (2010)

[11] Lucarini, V., Faranda, D., Wouters, J.: Universal behaviour of extreme value statistics for selected observables of dynamical systems. J. Stat. Phys. **147**(1),

63–73 (2012)

[12] Süveges, M.: Likelihood estimation of the extremal index. Extremes **10**(1-2), 41–55 (2007)

[13] Liebovitch, L.S., Toth, T.: A fast algorithm to determine fractal dimensions by box counting. Phys. Lett. A **141**(8-9), 386–390 (1989)

[14] Sarkar, N., Chaudhuri, B.B.: An efficient differential box-counting approach to compute fractal dimension of image. IEEE Transactions on systems, man, and cybernetics **24**(1), 115–120 (1994)

[15] Moloney, N.R., Faranda, D., Sato, Y.: An overview of the extremal index. Chaos **29**(2), 022101 (2019)

[16] Huang, B., Thorne, P.W., Banzon, V.F., Boyer, T., Chepurin, G., Lawrimore, J.H., Menne, M.J., Smith, T.M., Vose, R.S., Zhang, H.-M.: Extended reconstructed sea surface temperature, version 5 (ersstv5): upgrades, validations, and intercomparisons. Journal of Climate **30**(20), 8179–8205 (2017)

[17] Trenberth, K.E., Shea, D.J.: Atlantic hurricanes and natural variability in 2005. Geophy. Res. Lett. **33**(12) (2006)

[18] Anderson, T.W.: On the distribution of the two-sample cramer-von mises criterion. The Annals of Mathematical Statistics, 1148–1159 (1962)

[19] Ferrarin, C., *et al.*: Local and large-scale controls of the exceptional Venice floods of November 2019. Progress in Oceanography **197**, 102628 (2021)

[20] Umgiesser, G., *et al.*: The prediction of floods in Venice: methods, models and uncertainty (review article). Nat. Haz. and Earth Sys. Sci. **21**(8), 2679–2704 (2021)

[21] Lionello, P., *et al.*: Extreme floods of Venice: characteristics, dynamics, past and future evolution (review article). Nat. Haz. and Earth Sys. Sci. **21**(8), 2705–2731 (2021)

[22] Conte, D., Tiesi, A., Cheng, W., Papa, A., Miglietta, M.M.: Nowcasting of wind in the venice lagoon using wrf-fdda. Atmosphere **14**(3) (2023)

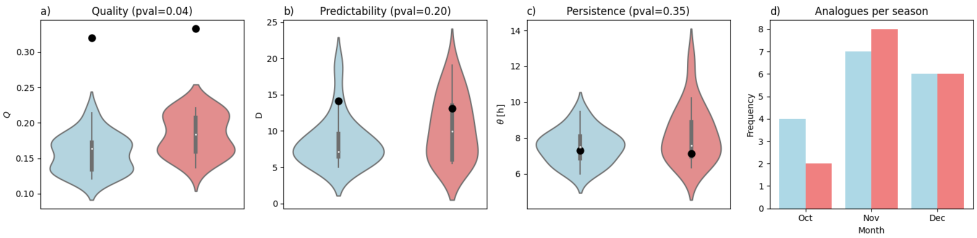

Supplementary Figure 1: Dynamical systems metrics Analysis for 1966 Acqua Alta event in Venice. Violin plots for past (blue) and present (rose) periods for analogues Quality Q (a) the Predictability index D (b), the Persistence index Θ (c) and the distribution of analogues in each month (d). Titles report the p-values of the Cramer-von Mises test. Values for the day of the extreme event are marked by a black dot.

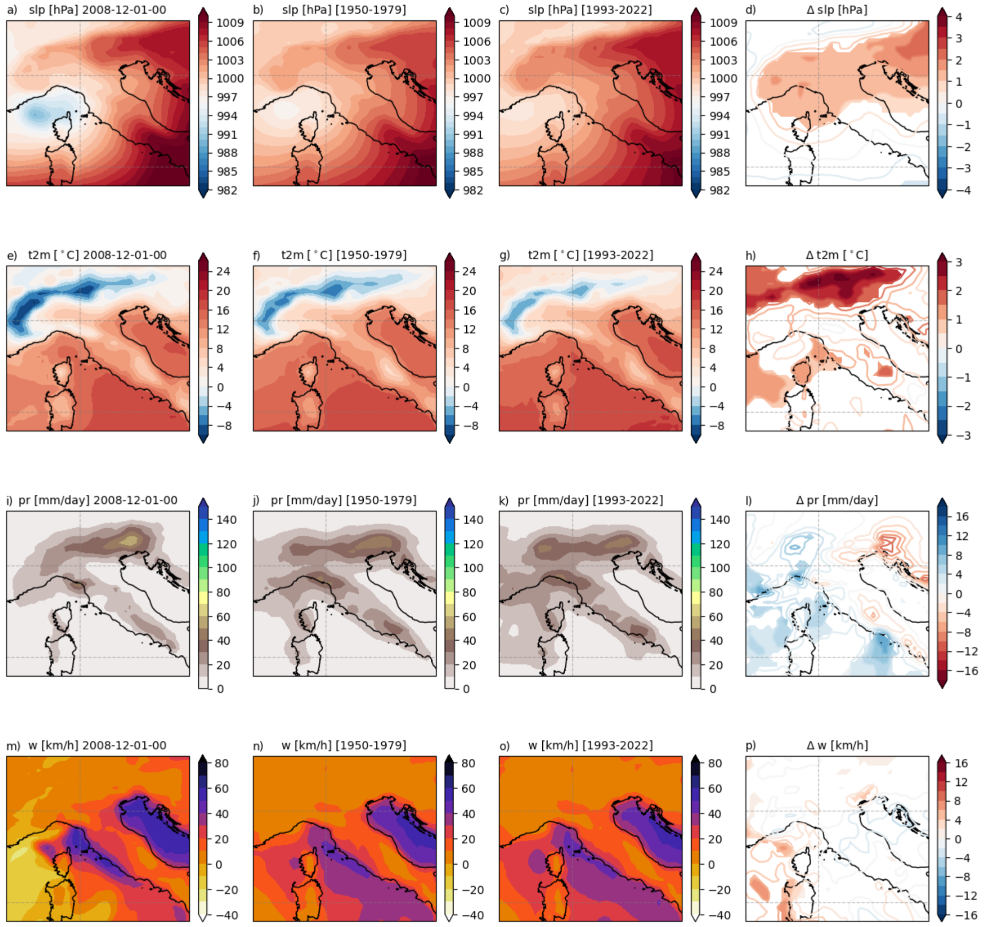

Supplementary Figure 2: Analogues Analysis for the 2008 Acqua Alta event in Venice. Daily mean sea-level pressure slp (a), 2-meter temperatures t2m (e), total precipitation tp (i), wind-speed wspd (m) on the day of the event at 00:00 UT. Average of the 17 sea-level pressure analogues found for the past [1950-1979] (b) and present [1993-2022] (c) periods and corresponding 2-meter temperatures (f,g), daily precipitation rate (j,k) and wind speed (n,o). Δslp (d), Δt2m (h), Δtp (i) and Δwspd (p) between present and past periods: colored-filled areas show significant anomalies with respect to the bootstrap procedure (significance level fixed as two standard deviation from the bootstrap mean).

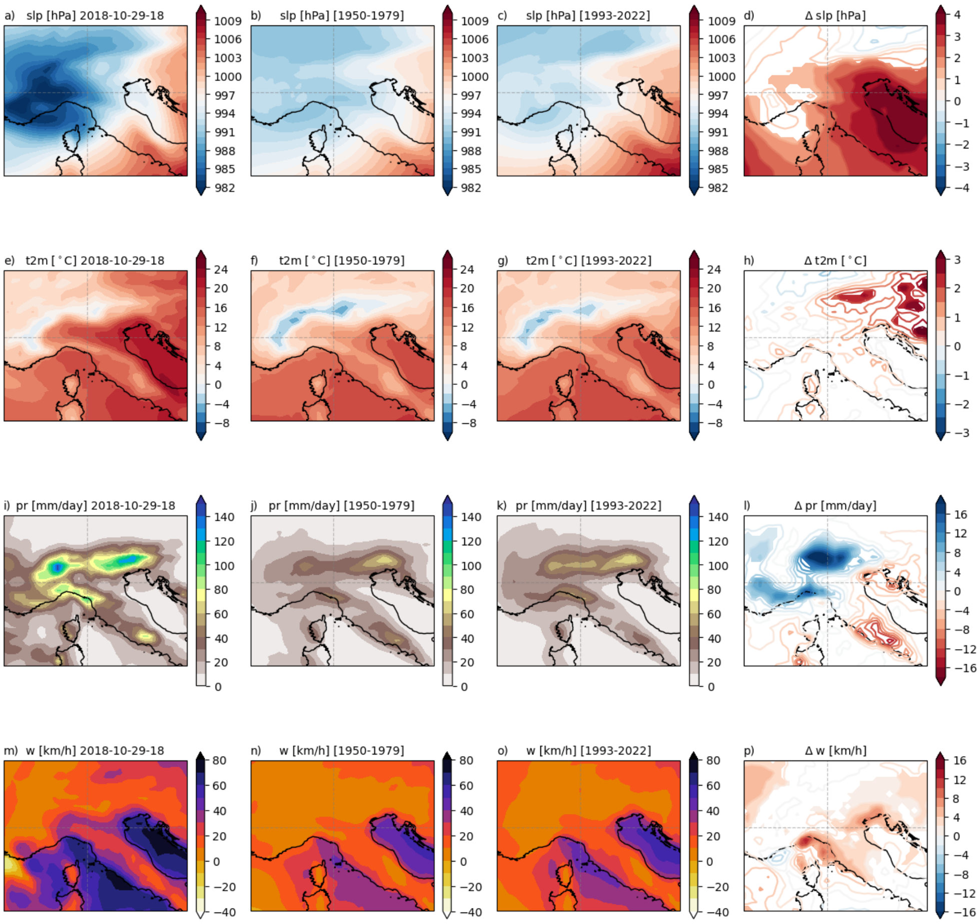

Supplementary Figure 3: Analogues Analysis for the 2018 Acqua Alta event in Venice. Daily mean sea-level pressure slp (a), 2-meter temperatures t2m (e), total precipitation tp (i), wind-speed wspd (m) on the day of the event at 18:00 UT. Average of the 17 sea-level pressure analogues found for the past [1950-1979] (b) and present [1993-2022] (c) periods and corresponding 2-meter temperatures (f,g), daily precipitation rate (j,k) and wind speed (n,o). Δslp (d), Δt2m (h), Δtp (i) and Δwspd (p) between present and past periods: colored-filled areas show significant anomalies with respect to the bootstrap procedure (significance level fixed as two standard deviation from the bootstrap mean).

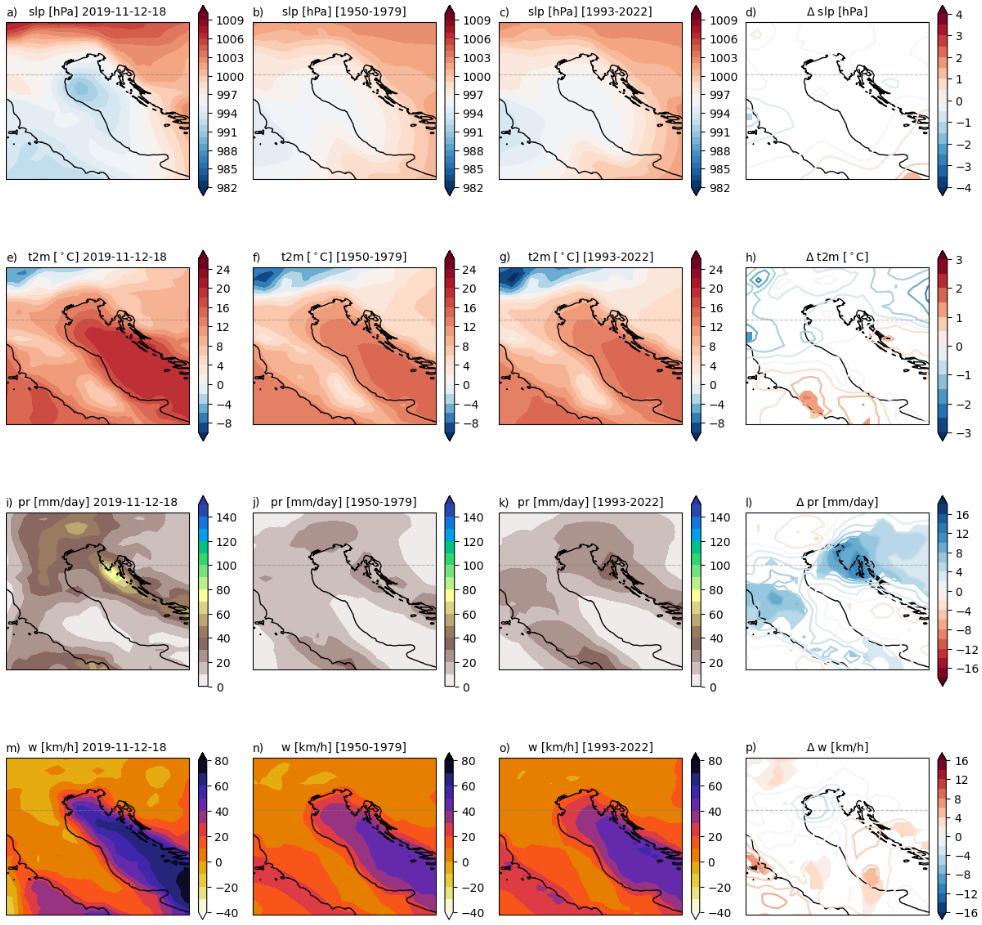

Supplementary Figure 4: Analogues Analysis for the 2019 Acqua Alta event in Venice. Daily mean sea-level pressure slp (a), 2-meter temperatures t2m (e), total precipitation tp (i), wind-speed wspd (m) on the day of the event at 18:00 UT. Average of the 17 sea-level pressure analogues found for the past [1950-1979] (b) and present [1993-2022] (c) periods and corresponding 2-meter temperatures (f,g), daily precipitation rate (j,k) and wind speed (n,o). Δslp (d), Δt2m (h), Δtp (i) and Δwspd (p) between present and past periods: colored-filled areas show significant anomalies with respect to the bootstrap procedure (significance level fixed as two standard deviation from the bootstrap mean).

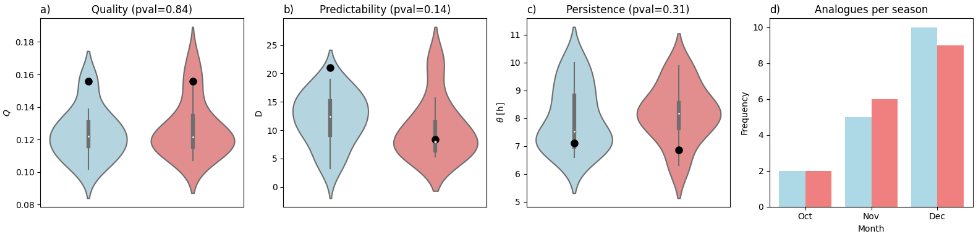

Supplementary Figure 5: Dynamical systems metrics for 2008 Acqua Alta event in Venice. Violin plots for past (blue) and present (rose) periods for analogues Quality Q (a) the Predictability index D (b), the Persistence index Θ (c) and the distribution of analogues in each month (d). Titles report the p-values of the Cramer-von Mises test. Values for the day of the extreme event are marked by a black dot

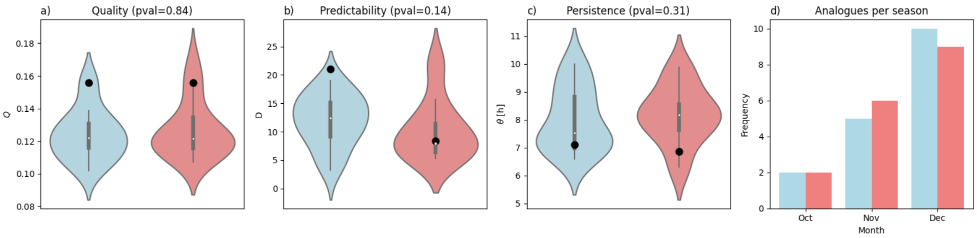

Supplementary Figure 6: Dynamical systems metrics for 2018 Acqua Alta event in Venice. Violin plots for past (blue) and present (rose) periods for analogues Quality Q (a) the Predictability index D (b), the Persistence index Θ (c) and the distribution of analogues in each month (d). Titles report the p-values of the Cramer-von Mises test. Values for the day of the extreme event are marked by a black dot

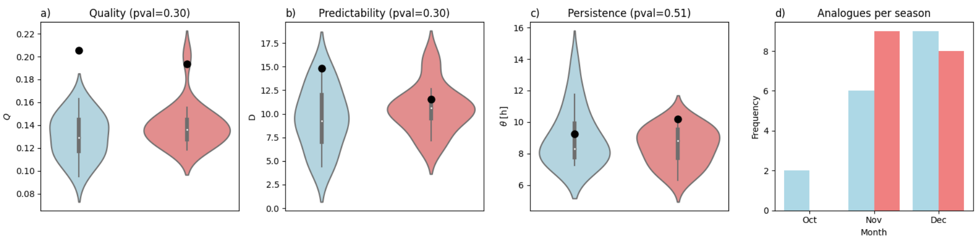

Supplementary Figure 7: Dynamical systems metrics for 2019 Acqua Alta event in Venice. Violin plots for past (blue) and present (rose) periods for analogues Quality Q (a) the Predictability index D (b), the Persistence index Θ (c) and the distribution of analogues in each month (d). Titles report the p-values of the Cramer-von Mises test. Values for the day of the extreme event are marked by a black dot

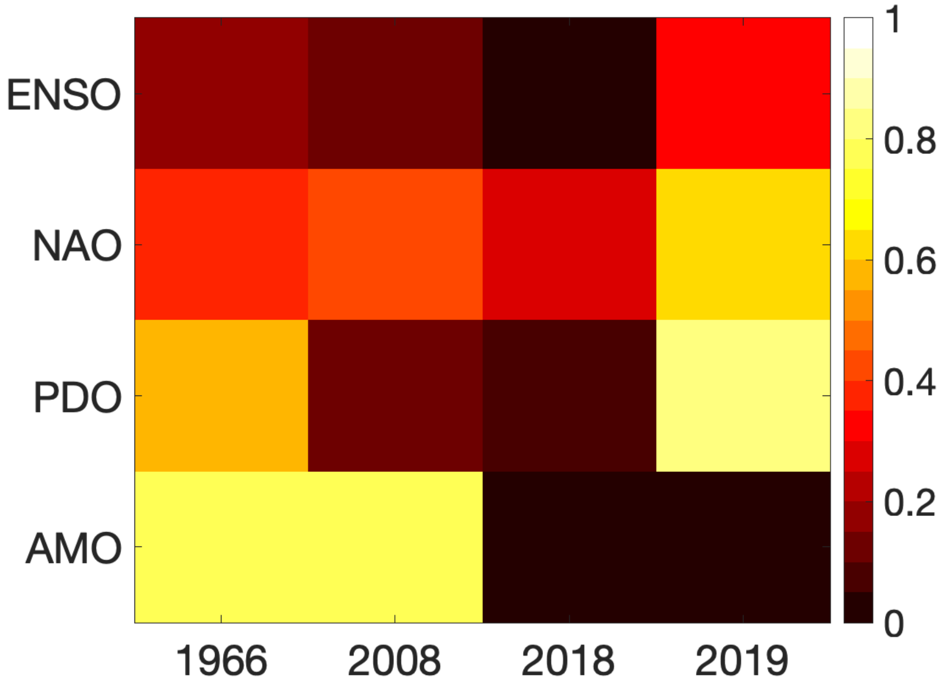

Supplementary Figure 8: Assessment of Natural Variability for all studied events. The p-values (colors) of the two-sided Cramér-von Mises test for the four different indices ENSO, NAO, PDO and AMO. If the p-value is smaller than 0.05, the null hypothesis that both samples are from the same distribution is rejected, namely we interpret the distributions as being significantly different. We use this test to determine the role of natural variability.

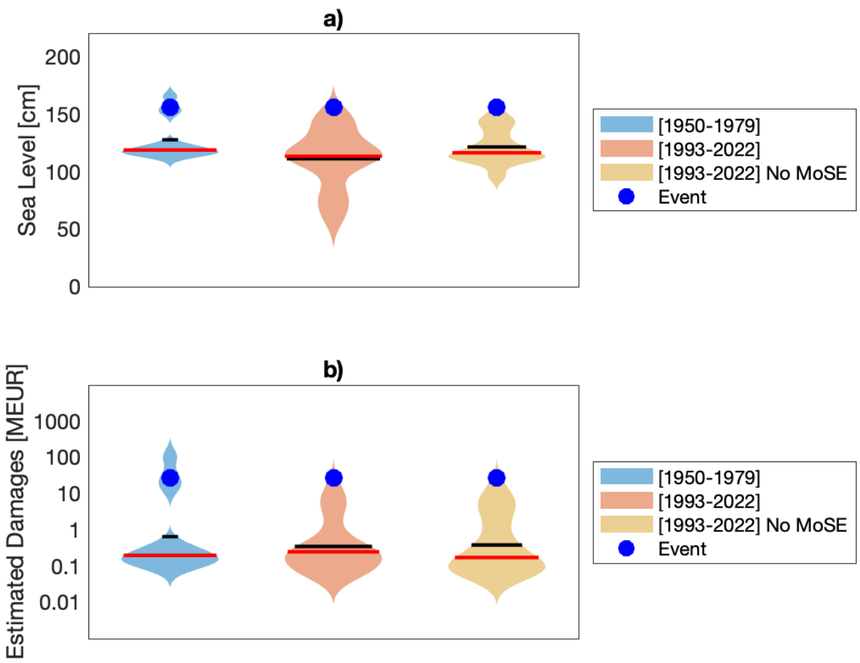

Supplementary Figure 9: Sea-levels SL during the analogues of the Acqua Alta 2008 event. SL for past (blue), present (orange) and counterfactual worlds without MoSE (ocre) (a), and estimated damages of the flooding events associated (b). In the violin plots, red (black) lines represent average (median) values.

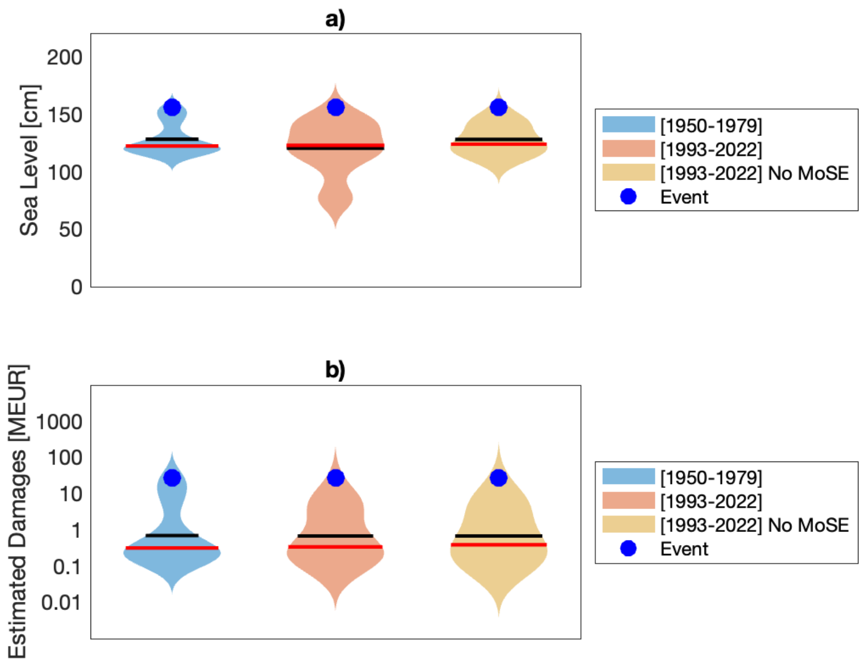

Supplementary Figure 10: Sea-levels SL during the analogues of the Acqua Alta 2018 event. SL for past (blue), present (orange) and counterfactual worlds without MoSE (ocre) (a), and estimated damages of the flooding events associated (b). In the violin plots, red (black) lines represent average (median) values.

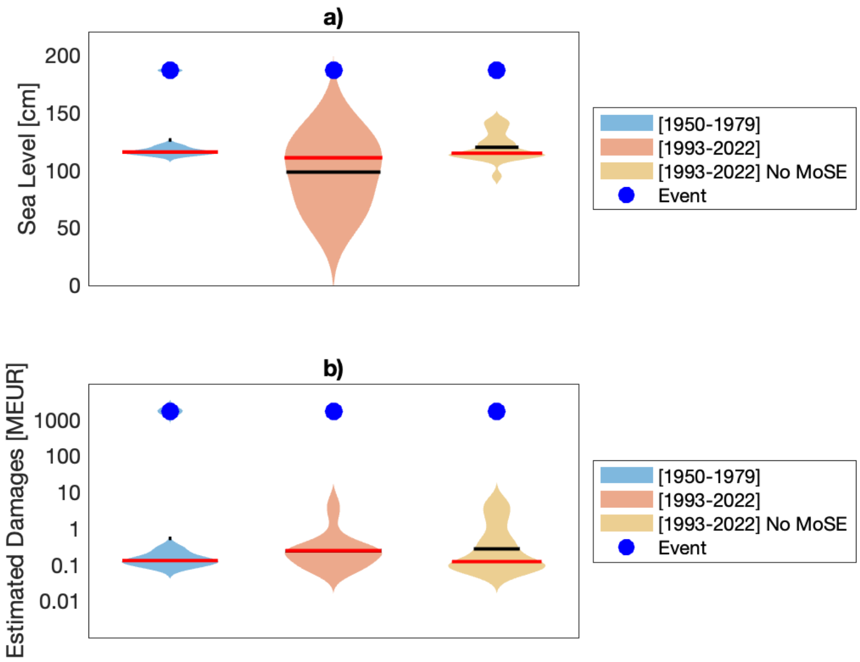

Supplementary Figure 11: Sea-levels SL during the analogues of the Acqua Alta 2019 event. SL for past (blue), present (orange) and counterfactual worlds without MoSE (ocre) (a), and estimated damages of the flooding events associated (b).In the violin plots, red (black) lines represent average (median) values.